Engineering Structures 166 (2018) 354–362

Contents lists available at ScienceDirect

Engineering Structures

journal homepage: www.elsevier.com/locate/engstruct

Composite box girder with corrugated steel webs and trusses – A new type of bridge structure

Yiyan Chen[b], Jucan Dong[a,b,*], Tianhua Xu[b,c]

[a] School of Civil Engineering, Hunan University, Changsha, China
[b] Shenzhen Municipal Design & Research Institute Co., Ltd., Shenzhen, China
[c] School of Civil Engineering, Shandong University, Jinan, China

ARTICLE INFO

Keywords:
Bridge engineering
Composite box girders
Corrugated steel webs
Trusses
Flexural capacity
Bridge design

ABSTRACT

Composite box girders with corrugated steel webs and trusses is a new type of advanced bridge structure proposed recently. This kind of structure consists of a top concrete slab, corrugated steel webs and two bottom concrete-filled steel tubes connected by trusses. The resistance to torsion and overturning of this kind of structure is larger than that of composite bridges with a single concrete-filled steel tube. This kind of structure is able to satisfy the requirement of rapid construction, environment protection and cost effectiveness. Two composite box girder bridges with corrugated steel webs and trusses have been or are being constructed in China. This paper presents the design of these two bridges in detail, which will provide valuable engineering experience for the further promotion of this kind of new bridge structure. Experimental research has been carried out to study the flexural behavior and the flexural capacity of this kind of new bridge structure. The test results show that when the test beam is at the elastic stage, the cross-section can be viewed as a plane section if only the strains of the concrete top slab and the bottom steel tubes are considered. The test beam shows good ductility throughout the whole loading process.

1. Introduction

The concrete box girder is one of the most commonly used structure forms for bridges because of its large flexural and torsional stiffnesses. However, with the increase of span length, the self-weight of a concrete box girder may increase rapidly, which restricts its use in long-span bridges [1]. One of the most promising ways to reduce the self-weight of bridges is to adopt steel–concrete composite structures. Nowadays, there are mainly three types of steel–concrete composite bridge structures: composite bridges with steel beams and top concrete slab, composite bridges with steel webs (or steel trusses) and top and bottom concrete slabs, and composite bridges with top concrete slab, steel trusses and bottom concrete-filled steel tube (Fig. 1(a)).

Among all the above mentioned types of composite bridges, the number of composite bridges with top concrete slab and bottom trusses is the smallest. This is because this kind of structure contains a lot of truss joints, and the fatigue and the stress concentration at such joints may lead to the failure at these locations before the global failure of the whole structure happens. That means the flexural capability of the bridge may not be fully utilized. To solve this problem, engineers proposed the composite bridge with Corrugated Steel Webs (CSWs) and Concrete-Filled Steel Tube (CFST, Fig. 1(b)), where the trusses are replaced by corrugated steel webs so that the number of joints can be greatly reduced. The Maupré Bridge [2] constructed in 1988 in France is the first bridge of this kind. Chen and Gao [3] has shown that such an improvement increases the ultimate flexural capacity of the bridge by nearly 80%. Meanwhile, the adoption of corrugated steel webs significantly improves the mechanical performance of the structure (e.g. [4,5]). This has been shown in the comprehensive studies on the mechanical performance of composite girders with CSWs and top and bottom concrete slabs, including the flexural behavior (e.g. [6–9]), the shearing behavior (e.g.[10–12]), the torsional behavior (e.g. [13,14]), the dynamic properties (e.g. [15,16]) and so on.

However, there are still some limitations in the composite bridge with CSWs and CFST (Fig. 1(b)). First, as the cross-section is triangular, the torsional stiffness and the resistance to overturning is relatively small. Second, the space for some construction procedures such as the welding between the corrugated steel webs and the steel tubes is limited. To further improve this kind of structure, the composite box girder with CSWs and trusses is proposed. Fig. 2 shows a typical cross-section of this kind of structure. The most important feature is that the single concrete-filled steel tube in Fig. 1(b) is replaced by two bottom steel

* Corresponding author at: School of Civil Engineering, Hunan University, Changsha, China.
E-mail address: dongjican@szmedi.com.cn (J. Dong).

https://doi.org/10.1016/j.engstruct.2018.03.047
Received 26 October 2017; Received in revised form 15 March 2018; Accepted 16 March 2018
Available online 04 April 2018

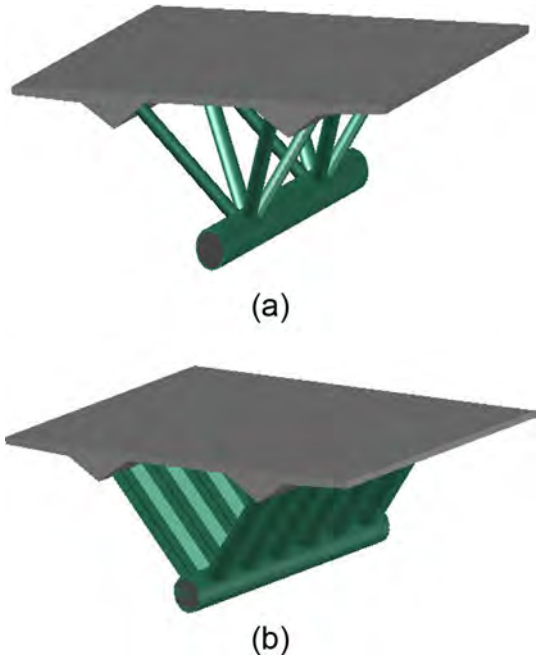

Fig. 1. Typical cross-section of (a) composite bridges with top concrete slab, trusses and bottom CFST; (b) composite bridges with CSWs and CFST.

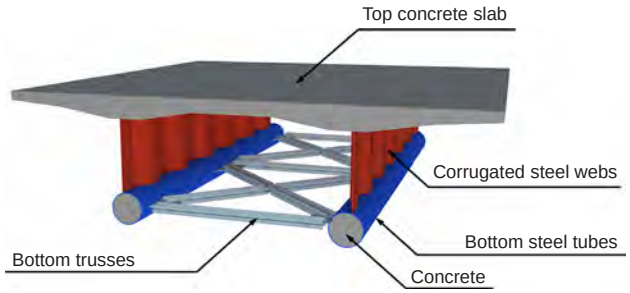

Fig. 2. Typical cross-section of composite box girders with CSWs and trusses.

tubes filled with concrete and connected by trusses, which may enhance the capability to resist torsion and overturning. The space for construction and maintenance within a bridge cross- section is also enlarged.

This paper aims to introduce to the public the composite box girder with CSWs and trusses, which is a new kind of composite bridge structure. In the following sections, a footbridge and a viaduct in China will be first presented in detail. Afterwards, the flexural behavior of this kind of bridge will be experimentally studied. The stress and strain characteristics and the failure mode under flexural loading will be summarized to provide a scientific basis for the application of this kind of bridge structure.

2. Engineering examples

2.1. A Footbridge in Hebei Province, China

The first composite box girder with CSWs and trusses that has been constructed is a footbridge located in Hebei Province, China, as shown in Fig. 3. It is a two-span simply supported girder bridge passing across the Beijing-Hong Kong-Macau Highway. This footbridge was designed by Shenzhen Municipal Design & Research Institute Co., Ltd.

The structural designs of the two spans of the footbridge are basically the same. Fig. 4(a)–(c) demonstrate the structural design of one of the spans of this footbridge. The net length of each span is 29.54 m. The depth of the girder is 1.60 m. The width of the top concrete slab is 3.30 m. The slope along the longitudinal direction of the bridge is 2.0%. At the bottom of the footbridge are two bottom steel tubes connected by horizontal trusses consisting of transversal and diagonal braces. The distance between the centers of the two bottom steel tubes is 1.50 m. Vertical trusses are also set up every 6.40 m along the longitudinal direction to enhance the integrity of the footbridge.

The typical cross-sections of the footbridge are shown in Fig. 4(d). The footbridge is a single-box structure. The thickness of the top concrete slab is 0.15 m at the edge and at the center of the cross-section, and 0.30 m at the intersection with corrugated steel webs. Both the horizontal and the vertical trusses are made of steel tubes. The diameters of the tubes at the horizontal and the vertical trusses are 168 and 146 mm, respectively. The thickness of these steel tubes is 6 mm. The diameter and the thickness of the bottom steel tubes are 500 and 24 mm, respectively. All steel tubes are made of Chinese standard

Fig. 3. A footbridge at Hebei Province, China.

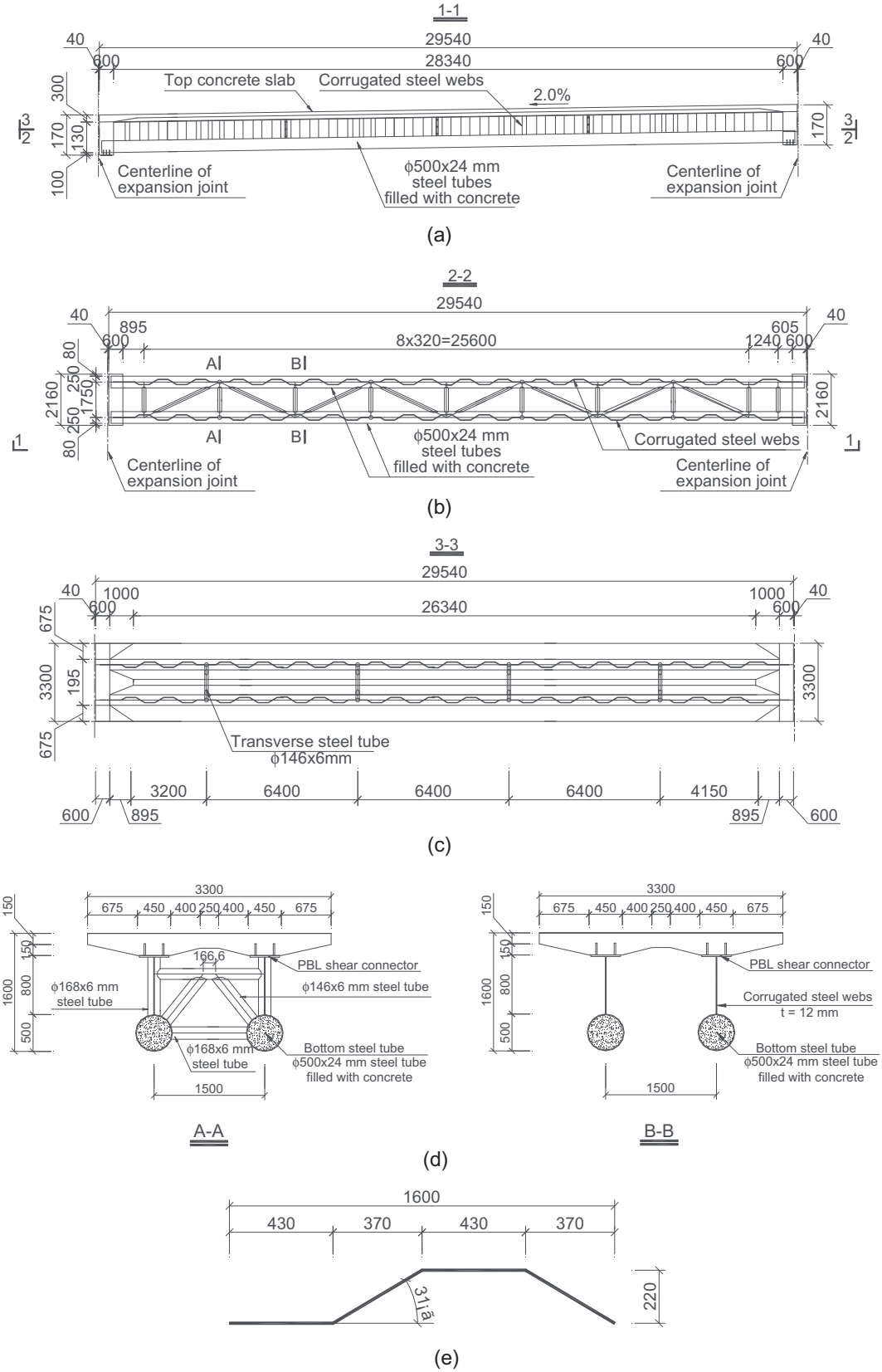

Fig. 4. Design of the footbridge (Unit: mm): (a) side view (Section 1–1); (b) Section 2–2; (c) Section 3–3; (d) typical cross-sections; (e) a corrugation of webs.

Q345D steel with a minimum yielding strength and ultimate strength of 345 MPa and 490 MPa, respectively. Both the two bottom steel tubes are filled with concrete with a compressive strength larger than 50 MPa. Fig. 4(e) shows a corrugation of the corrugated steel webs of the footbridge. The length and height of the corrugation are 1600 and 220 mm, respectively. The thickness of the webs is 12 mm. The corrugated steel webs are connected with the top concrete slabs by perfobond strip (PBL) connectors. For the connection between the corrugated

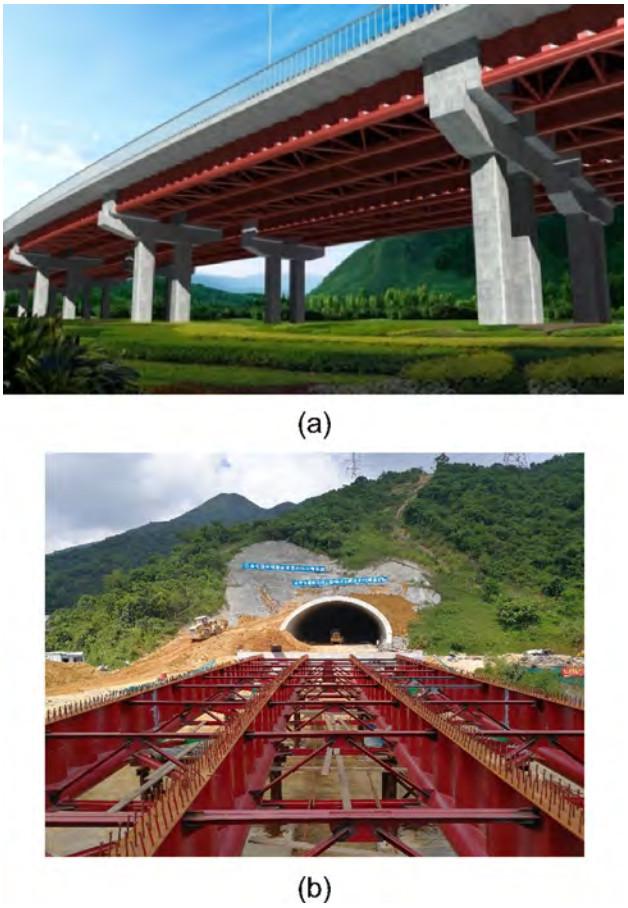

Fig. 5. Maluanshan Park Viaduct: (a) architectural rendering; (b) construction site.

steel webs and the end diaphragms, holes were first drilled on the corrugated steel webs and then steel reinforcement bars were extended through the holes.

In this footbridge, the bottom steel tubes were embedded into the end diaphragm to get a good connection between each other. On the surface of the embedded part of the steel tubes, 50 mm-long studs were welded with an interval of 100 mm to enhance the bonding between the steel tube surface and the concrete. Holes with diameters of 22 mm were first drilled at the end steel plates of the bottom steel tubes. Then six steel reinforcement bars were extended through the holes into the concrete inside the bottom steel tubes. With these arrangements, the concrete at the end diaphragm and that inside the bottom steel tubes was able to be well united and work together under external loadings.

2.2. Maluanshan Park Viaduct in Shenzhen, China

Another bridge of this type that is being constructed is the Maluanshan Park Viaduct in Shenzhen, Guangdong Province, China. Several important factors were considered when designing the viaduct. First, it passes over a reservoir used for water supply, hence the influence of the bridge construction on the surrounding environment should be minimized. For example, the bridge should be constructed without the intensive use of temporary braces. Second, the bridge should also blend with the surrounding landscape. Finally, the bridge should be constructed rapidly, and the cost should not be too high. After careful consideration, it was decided to adopt the composite box girder with CSWs and trusses for this viaduct. The architectural rendering and the construction site of the viaduct are shown in Fig. 5. The viaduct is designed under the standard for an urban highway with a design speed of 80 km/h. The design of the Maluanshan Park Viaduct was also carried out by Shenzhen Municipal Design & Research Institute Co., Ltd.

The Maluanshan Park Viaduct includes a left and a right sub-bridges. The left sub-bridge is a 45.00 m simply supported girder bridge, while the right sub-bridge is a 3 × 45.00 m continuous girder bridge. The width of each of the two sub-bridges is 20.00 m. The two sub-bridges are both two-box one-cell structures.

The left sub-bridge is used as an example here to show the design of the viaduct in detail. The depth of the girder is 2.80 m. Two end diaphragms are set up at the support locations. The depth and thickness of the end diaphragms are 3.00 and 1.20 m, respectively. Fig. 6(a) and (b) shows the typical cross-sections of the left sub-bridge. It is comprised of two boxes, and each box consists of one single cell. The width of the top concrete slab is 20.00 m. The width of the cantilever part of the top concrete slab is 2.80 m. The thickness of this cantilever part varies from 0.20 m at the free end to 0.50 m at the intersection with the corrugated steel webs. One traffic lane of 16.00 m wide and two lanes for bridge maintenance of 2.00 m wide are set on the left sub-bridge. The transverse slope of the top surface of the top concrete slab is 2.0%. The width of the bottom of a box at the cross-section is 4.80 m.

As shown in Fig. 6(c), two steel tubes connected by trusses are

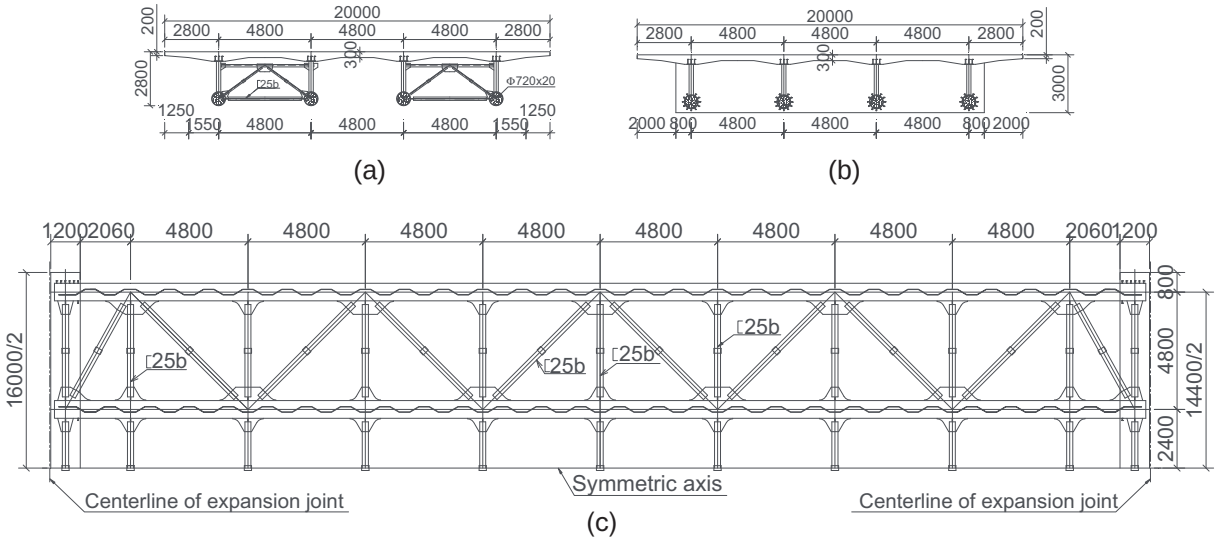

Fig. 6. Design of the left sub-bridge of the Maluanshan Park Viaduct (Unit: mm): (a) cross-section at the mid-span; (b) cross-section at a support; (c) arrangement of bottom truss structure.

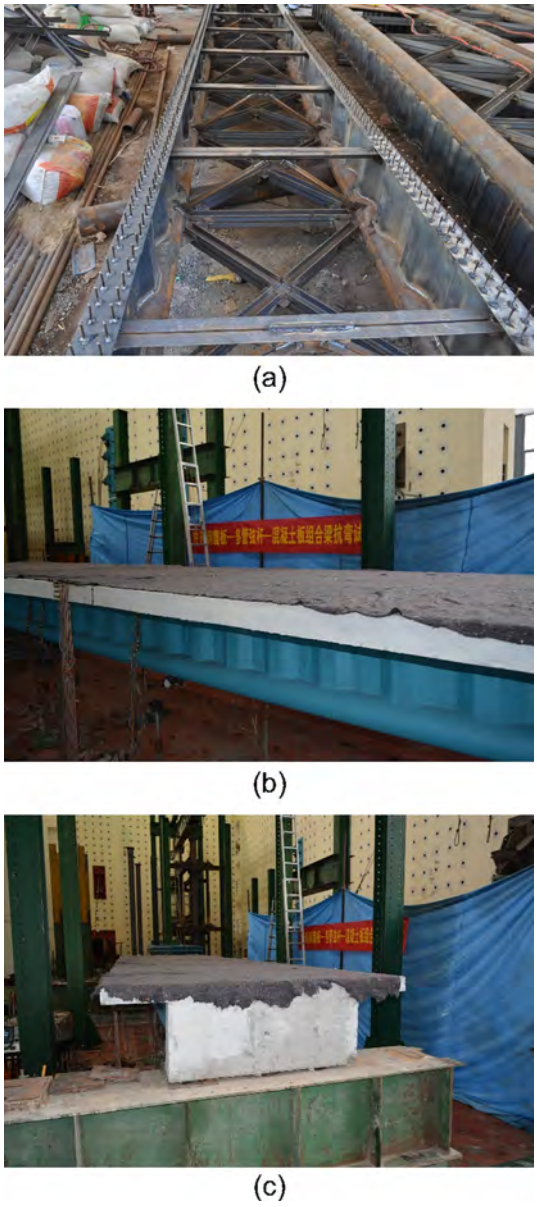

Fig. 7. Test beam under construction.

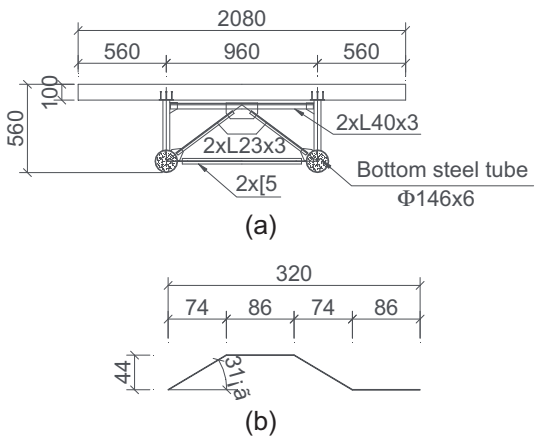

Fig. 8. (a) Typical cross-section; and (b) a corrugation of the webs of test beam (Unit: mm).

placed at the bottom of each box structure. The diameter and the thickness of the tubes are 720 and 20 mm, respectively. The tubes are filled with slightly expansive concrete. The compressive strength of the concrete is larger than 50 MPa. The trusses connecting the steel tubes are comprised of transverse and diagonal braces. Each of these braces was made of a steel channel with trapezoidal steel plates welded to its both ends. The trapezoidal steel plates were then welded to the bottom concrete-filled steel tubes. To enhance the torsional performance of the bridge, nine vertical trusses are placed with a 9.00 m interval along the longitudinal direction.

The corrugated steel webs used in the Maluanshan Park Viaduct are made of Chinese standard Q345qC steel. The minimum yielding stress and the tensile strength are 345 and 490 MPa, respectively. The corrugation is the same with that of the footbridge introduced in the previous section (Fig. 4(e)). Stud connectors are used to connect the corrugated steel webs and the top concrete slab.

Considering the viaduct is a larger scale structure than a footbridge, the connection between the bottom steel tubes and the end diaphragms in the Maluanshan Park Viaduct is made stronger than that in the previous case. The bottom steel tubes were embedded into the end diaphragm. Studs with a diameter of 22 mm and a length of 100 mm were welded on the surface of the embedded part to enhance the bonding between the steel tubes and the concrete. A horizontal brace made of a steel channel is used to connect the steel tubes near their ends and then also embedded into the end diaphragms. With this arrangement, the integrity of the end diaphragm can be strongly improved, and the ends of the bottom steel tubes is waived from unfavorable stress states.

The right sub-bridge of the Maluanshan Viaduct is a three-span continuous girder bridge. The structural design of the right sub-bridge is almost the same as that of the left sub-bridge, and therefore not introduced in detail here. One of the differences between the two sub-bridges is that internal pre-stressed tendons have to be installed within the top concrete slab of the right sub-bridge to withstand the negative bending moment at the areas near the supports. Totally 48 tendons with a diameter of 15.24 mm are utilized. The tensile strength of the tendons (f_{pk}) used in design is 1860 MPa, and the elastic modulus of the tendons is 1.95×10^5 MPa. The jacking prestress is 1339 MPa (0.72 f_{pk}).

Considering the viaduct is located in a subtropical coastal humid area, all the steel structural members are carefully coated to prevent rust and corrosion. The designed service life of such coating is 15–25 years.

Comparison has been made among several possible bridge structure types that can be adopted for the Maluanshan Park Viaduct. The result shows that the construction cost for bridges with truss structures is 50% higher, while the construction cost for the structure presented in this section is only 30% higher than that of conventional concrete box girder bridges.

3. Experimental research on flexural behavior of composite box girders with CSWs and trusses

As a new kind of bridge structure, the mechanical performance of composite box girders with CSWs and trusses has yet to be investigated. Considering flexural behavior is one of the most important factors considered in the design of girder bridges, experimental research has been first carried out to preliminarily investigate the flexural behavior of composite box girders with CSWs and trusses.

3.1. Details of test beam

In this research, a scaled model of the Maluanshan Park Viaduct with a linear dimension scale factor (S_l) of 1/5 was designed and constructed for the experimental study. Fig. 7 shows the test beam under construction. The span length of the test beam, which is corresponding to the distance between the centerlines of two adjacent expansion joints

Table 1
Material properties obtained from laboratory tests.

Materials	Location	Young's modulus (MPa)	Compressive strength (MPa)	Yielding strength (MPa)	Ultimate tensile strength (MPa)
Concrete	Top slab	3.96×10^4	53.0	–	–
	Inside bottom steel tubes	3.68×10^4	49.5	–	–
Steel	Bottom steel tubes	2.03×10^5	–	316	419
	Corrugated steel webs	2.47×10^5	–	332	426

Table 2
Scale rule of modeling test.

Quantity	Scale factor
Stress	1
Strain	1
Modulus	1
Poisson's ratio	1
Linear dimension	S_l
Displacement	S_l
Area of reinforcement	S_l^2
Concentrated load	S_l^2
Line load	S_l
Pressure	1

Note: $S_l = 1/5$ in the experimental research reported in this paper.

at the reference viaduct, is 9000 mm. The actual length of the test beam is 8984 mm, and the distance between the centerlines of two end supports is 8740 mm. The depth and width of the beam are 560 and 2080 mm, respectively. The typical cross-section of the test beam is shown in Fig. 8(a). Such a cross-section consists of a top concrete slab and two bottom steel tubes connected by trusses. The thickness of the top concrete slab is 100 mm. The diameter of each bottom steel tube is 146 mm, and the thickness of the tube wall is 6 mm. The steel tubes were filled with concrete. Fig. 8(b) shows a corrugation of the corrugated steel webs of the test beam. The thickness of the corrugated steel webs is 4 mm, and the length and height of a corrugation are 320 and 44 mm, respectively. The corrugation angle is 31°. Longitudinal and transverse steel reinforcement bars with a diameter of 12 mm were placed inside the top concrete slab and the end diaphragms forming reinforcement nets. Table 1 lists the material properties obtained from laboratory tests.

3.2. Loading set up and instrumentation

The loads applied to the test beam were determined by scaling the designed loads of the reference viaduct according to the scale rules of modeling tests [17] (Table 2) so that the resultant stress and strain of the test beam and the reference viaduct can be the same. During the test, two layers of concrete blocks (total height = 760 mm) were first placed on the top surface of the test beam to simulate the dead load. The live loads were simulated by applying a concentrated load of 30 kN at each of the $x = L/3$ and $x = 2L/3$ locations of the test beam (where x is the coordinate along the longitudinal direction, and L is the span of the test beam). The concentrated loads in the test were applied using a loading device comprised of two actuators with a capacity of 1000 kN and two reaction frames. A steel transfer beam was used to distribute the load at each of the two prescribed loading locations. Fig. 9 shows the overview of the test setup.

To measure the deflection of the test beam, 10 Linear Variable Displacement Transducers (LVDTs) were installed at the locations shown in Fig. 10. The LVDTs located at the two ends of the test beam were used to measure the settlement of the supports. The deformation of the top concrete slabs, the corrugated steel webs and the bottom steel tubes were measured by strain gauges set at the locations demonstrated in Fig. 10(a). Moreover, the steel reinforcement bars in the top concrete

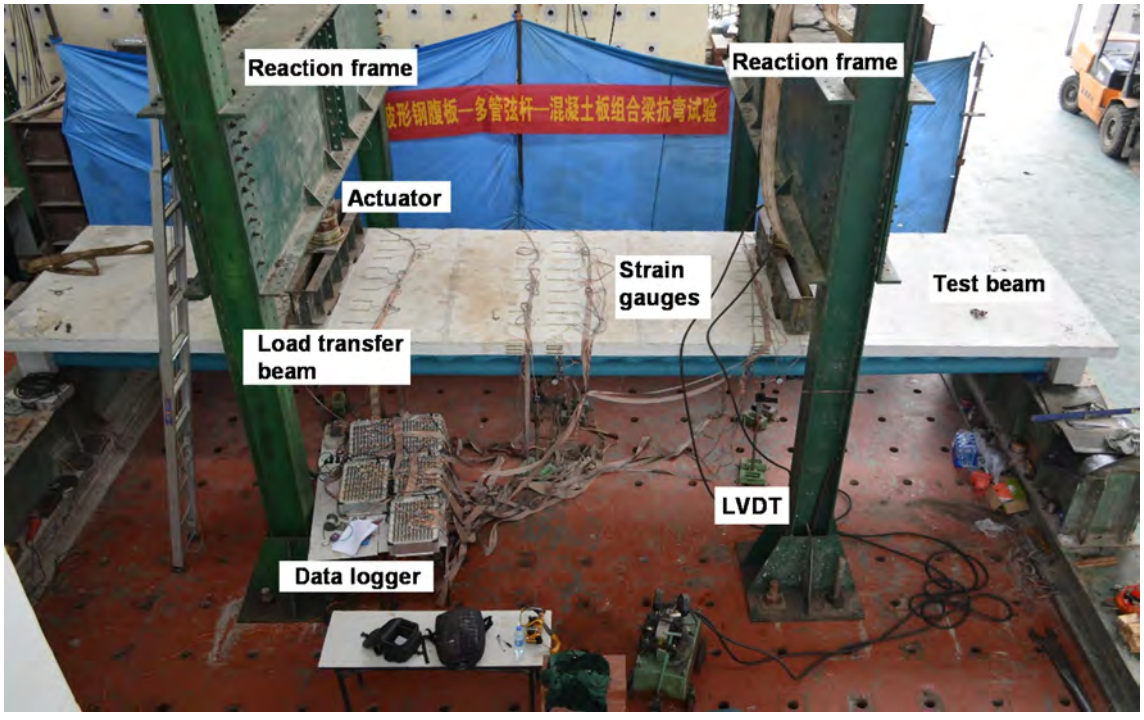

Fig. 9. Overview of test set up.

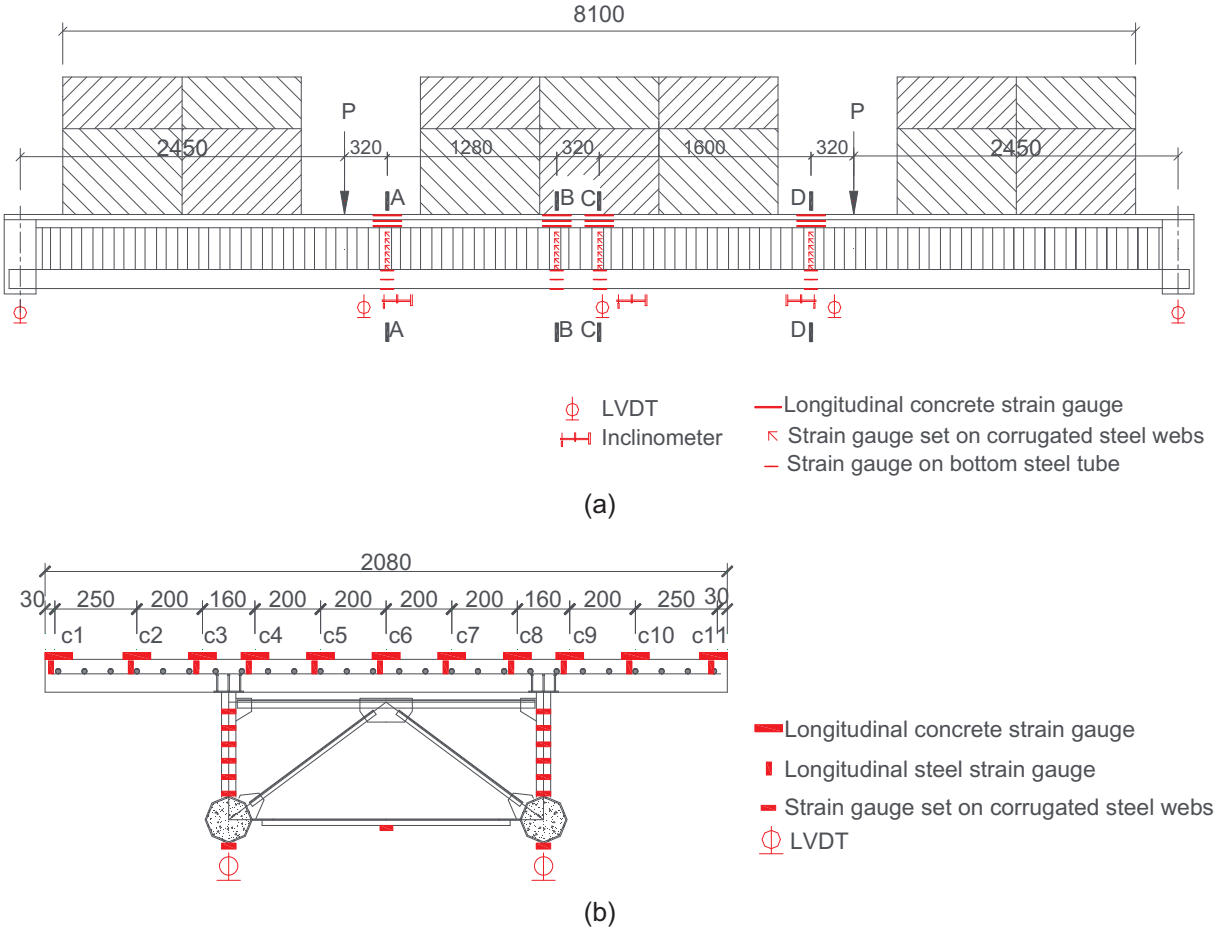

Fig. 10. Loading set up and instrumentation of the test beam (Unit: mm): (a) side view; (b) typical cross-section.

slabs were also equipped with strain gauges. The arrangement of strain gauges and LVDTs at a typical cross-section of the test beam is shown in Fig. 10(b).

3.3. Test procedures

Before the flexural test, a pre-loading force equal to 10% of the estimated ultimate flexural capacity was first applied to the test beam. The pre-loading force was kept for 3 min and then the test beam was unloaded.

The test was carried out under a force control process. The external loading was applied to the test beam step by step. When the test beam was at an elastic stage, the loading was increased by 10 kN and then kept for 3 min at each step. After the test beam reached an elasto-plastic stage, the loading increased at each step was reduced to 5 kN. When the beam was close to its failure state, the test load was slowly and continuously applied. The test ended after the test beam failed.

To ensure the safety of the test, the test beam is regarded as failed when one of the following conditions is satisfied. (1) The deflection at the mid-span of the test beam is larger than 1/50 of the span length (which is 180 mm for the test beam in this research). (b) The longitudinal normal strain of the bottom concrete-filled steel tube is larger than 30,000 με, which means that the tube has fully yielded. (c) The corrugated steel webs or the bottom steel tubes buckles, or local failure of the test beam occurs. (d) Cracks of more than 5 mm wide occurs at the bottom of the top concrete slab, or the top concrete slab is crushed.

3.4. Results and analysis

Fig. 11 shows the observed failure mode of the test beam. The deflection at the mid-span cross-section was 199.7 mm, which exceeds 1/50 of the span length of the test beam. Transverse cracks were observed at the bottom of the top concrete slab, as shown in Fig. 11(b). The materials in the test beam had reached their yield strength before it failed. Neither local buckling of corrugated steel webs nor local failures of structural elements have been observed.

Fig. 12 shows the measured load–deflection curve of the test beam. According to the curve, the test beam shows good ductility. The deformation of the test beam can be divided into four stages based on the deflection and the strains at the mid-span.

(a) Elastic stage (*OA*)

The very first stage of deformation is an elastic stage in which the deflection increased almost linearly with the flexural load. Point *A* in Fig. 12 is defined as the ending point of this stage because at this point the longitudinal normal strain of the bottom of the bottom steel tube reached its proportional limit strain (1042 με). The deflection of the test beam at this stage was small, which is only 1/450 of the span length.

(b) Elasto-plastic stage (*AB*)

The stage following the elastic stage is regarded as an elasto-plastic stage where the bottom steel tubes started to yield by tension and the load–deflection curve became nonlinear. At the ending point of this stage, Point *B* in Fig. 12, the longitudinal normal strain of the top of the

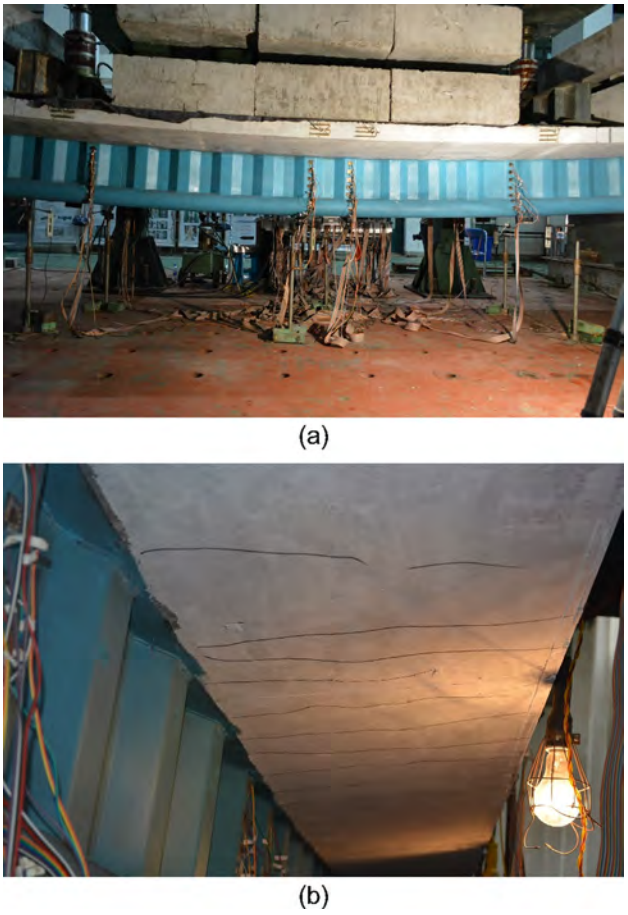

Fig. 11. Failure mode of the test beam: (a) overview; (b) observation at the bottom of the top concrete slab.

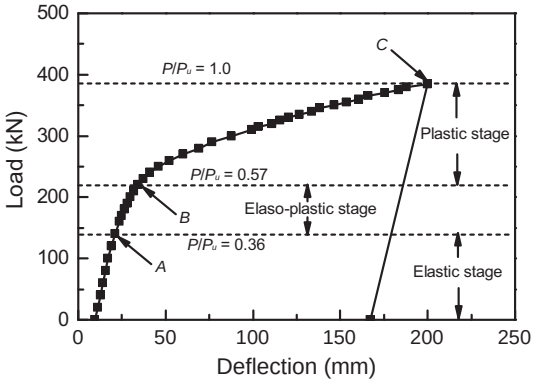

Fig. 12. Load-deflection curve measured at mid-span of test beam.

bottom steel tube achieved the yielding strain (1558 με). The deflection of the test beam at Point *B* is 1/300 of the span length.

(c) Plastic stage (*BC*)

At this stage, the deflection increased rapidly with the flexural load. Cracks started to occur at the bottom of the top concrete slab when the test load was 270 kN, indicating that the neutral axis of the cross-section has shifted to within the top concrete slab. When the test load reached 385 kN, the cracks extended upward from the bottom of the concrete slab to a height of 1/3 of the slab thickness. Deformations of the test beam at this moment were visibly perceptible to the researchers. The deflection at the mid-span was 199.7 mm (1/46 of the

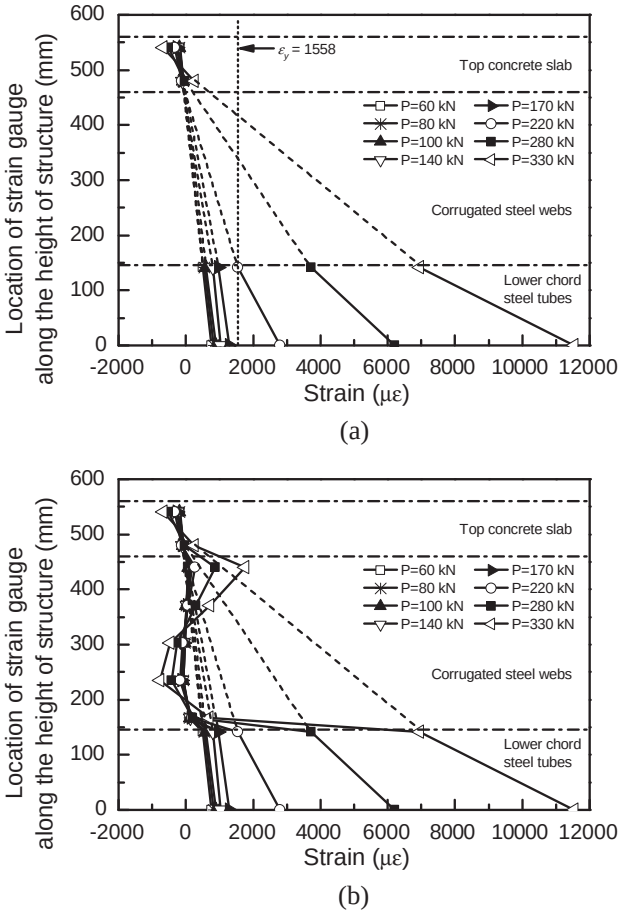

Fig. 13. Longitudinal normal strains of (a) the top concrete slab and the bottom steel tubes; and (b) the corrugated steel webs.

span length), and therefore it was regarded as failed and the ultimate load was correspondingly determined as 385 kN.

(d) Unloading stage

The test beam was unloaded after it failed. Before unloading, the longitudinal strains at the top and bottom of the bottom steel tubes were 11,974 and 15,950 με, respectively. The residual deflection at the middle of the span was 167.3 mm.

The distribution of the longitudinal normal strain of the top concrete slab and the bottom steel tubes along the height at different load steps are shown in Fig. 13(a). At the elastic stage ($\varepsilon < \varepsilon_y$), the measured strain data points can be approximately connected by a straight line, indicating that the cross-section can be approximated as a plane section when only the top concrete slab and the bottom steel tubes are concerned. When the strain exceeds the yielding strain ε_y, the data points can no longer be connected by a single straight line, so the assumption of plane section remaining plane seems not valid at this stage. Fig. 13(b) shows the longitudinal strain of the corrugated steel webs. If the corrugated steel webs are considered, the assumption that “plane sections remain plane” is no longer valid. At the elastic deformation stage, the strain of the corrugated steel webs is small compared with those of the concrete top slab and the bottom steel tubes. Therefore, the flexural load is mainly sustained by the top concrete slab and the bottom steel tubes.

3.5. Comparison with real bridge

The Maluanshan Park Viaduct was designed following *General*

Specifications for Design of Highway Bridges and Culverts (JTG D60-2015) [18] in China. According to this design specification, when a bridge is designed according to the ultimate limit state, the design values of the effect of loadings, S_{ud}, should be calculated by

$$S_{ud} = \gamma_0 S\left(\sum_{i=1}^{m} \gamma_{Gi} G_{ik}, \gamma_{Q1}\gamma_L Q_{1k}, \psi_c \sum_{j=2}^{n} \gamma_{Lj}\gamma_{Qj} Q_{jk}\right) \quad (1)$$

where $S()$ is the effect of the loadings included in the bracket; γ_0 is the importance factor for the structure; γ_{Gi}, γ_{Q1} and γ_{Qj} are the load factors for the ith permanent loadings, the vehicle loading and the jth variable loading, respectively; γ_L and γ_{Lj} are the coefficients related to the designed service period of the structure for the vehicle loading and the jth variable loading, respectively; G_{ik} is the standard value of the ith permanent loading; Q_{1k} is the standard value of the vehicle loading; Q_{jk} is the standard value of the jth variable loading.

For the test beam in this research, the values of the load factors follow those for the Maluanshan Park Viaduct, i.e. $\gamma_0 = 1.1$, $\gamma_{Gi} = 1.2$ and $\gamma_{Q1} = 1.4$. According to the measurement during the test, the bending moment at the middle of the test beam span corresponding to the simulated permanent and variable loadings are 333 kN·m and 73.5 kN·m, respectively. Therefore, $\gamma_0 M_d = 1.1 \times (1.2 \times 333 + 1.4 \times 73.5) = 552.8$ kN·m. The measured bending moment at the middle of the test beam span corresponding to the elastic limit and the ultimate states are $M_e = 599.3$ kN·m and $M_u = 1199.5$ kN·m, respectively. Therefore, $\gamma_0 M_d/M_e = 0.92$, and $\gamma_0 M_d/M_u = 0.46$, indicating that the test beam is within the elastic limit and far from failure when only the permanent and variable loadings of the viaduct are simulated. As the experiment is designed following the scale rule of modeling tests, the mechanical performance of the test beam represents that of the real viaduct. Therefore, based on the experimental results, the Maluanshan Park Viaduct will work within the elastic limit when it is subjected to the permanent and variable loadings specified in the design guideline. The composite box girder with CSWs and trusses can be a promising bridge structure for use in practice.

4. Summary and conclusion

In this paper, the composite box girder bridge with CSWs and trusses has been introduced. Two engineering examples, including a footbridge and a viaduct, have been demonstrated in detail. The flexural behavior of this kind of structure has been experimentally investigated. The following conclusions can be drawn for the current paper.

(1) The composite box girder with CSWs and trusses is a newly proposed bridge structure. With the use of corrugated steel webs and bottom trusses, the self-weight of the structure can be minimized. The consumed material and the cost for the bridge construction are reduced, and the bridge construction and maintenance can be simplified. The use of this kind of bridge may satisfy the requirement of rapid construction and cost saving, therefore it is worth being promoted around the world.
(2) According to the experimental research on a scaled model of the Maluanshan Park Viaduct, this kind of structure shows good ductility and integrity under flexural load when it is properly designed. The flexural deformation can be divided into an elastic stage, an elasto-plastic stage and a plastic stage. At the failure stage, the neutral axis of the cross-section may shift to within the top concrete slab, generating transverse cracks on the bottom of the slab.
(3) The longitudinal normal strain of the corrugated steel webs is small at the elastic and the elasto-plastic stages, indicating that the flexural loading is mainly sustained by the top concrete slab and the bottom trusses. The assumption that “plane sections remain plane” is not valid for the whole cross-section. However, the cross-section may still be regarded as a plane section at the elastic stage when only the top concrete slab and the bottom steel tubes are considered.
(4) Experimental results show that the Maluanshan Park Viaduct will work within the elastic limit when it is subjected to the permanent and variable loadings specified in the design guideline.

Acknowledgements

This work was supported by the National Natural Science Foundation of China (Project No. 51578323), Guangdong Provincial Department of Science and Technology (Project No. 2012-02-025) and Science and Technology Innovation Committee of Shenzhen (Project No. JCYJ20140902162220208).

References

[1] Rosignoli M. Prestressed concrete box girder bridges with folded steel plate webs. Proc ICE-Struct Build 1999;134(1):77–85.
[2] Combault J. The Maupré Viaduct near Charolles, France. In: Proceeding of the 1988 national steel construction conference, Miami; 1988.
[3] Chen BC, Gao J. Experimental studies on concrete filled steel tubular beam with corrugated steel web under bending. J Build Sci, 2008;29(1):75–82 (in Chinese).
[4] Sayed-ahmed EY. Behaviour of steel and (or) composite girders with corrugated steel webs. Can J Civ Eng, 2001;28(4):656–72.
[5] Jiang RJ, Au FTK, Xiao YF. Prestressed concrete girder bridges with corrugated steel webs: review. J Struct Eng ASCE 2015;141(2):04014108.
[6] Elgaaly M, Seshadri A, Hamilton RW. Bending strength of steel beams with corrugated webs. J Struct Eng 1997;123(6):772–82.
[7] Chan CL, Khalid YA, Sahari BB, Hamouda A. Finite element analysis of corrugated web beams under bending. J Constr Steel Res 2002;58(11):1391–406.
[8] Chen XC, Au FT, Bai Z, Li Z, Jiang R. Flexural ductility of reinforced and prestressed concrete sections with corrugated steel webs. Comput Concr 2015;16(4):625–42.
[9] Chen XC, Bai Z, Zeng Y, Jiang R, Au FT. Prestressed concrete bridges with corrugated steel webs: Nonlinear analysis and experimental investigation. Steel Compos Struct 2016;21(5):1045–67.
[10] He J, Liu Y, Lin Z, Chen A, Yoda J. Shear behavior of partially encased composite I-girder with corrugated steel web: numerical study. J Constr Steel Res 2012:166–82.
[11] Hassanein MF, Kharoob OF. Behavior of bridge girders with corrugated webs: (II) shear strength and design. Eng Struct 2013;57:544–53.
[12] Hassanein MF, Kharoob OF. Shear buckling behavior of tapered bridge girders with steel corrugated webs. Eng Struct 2014;74:157–69.
[13] Mo YL, Jeng CH, Chang YS. Torsional behavior of prestressed concrete box-girder bridges with corrugated steel webs. ACI Struct J 2000;97(6):849–59.
[14] Ding Y, Jiang KB, Liu YW. Nonlinear analysis for PC box-girder with corrugated steel webs under pure torsion. Thin-Walled Struct 2012;51:167–73.
[15] Mo YL, Jeng CH, Krawinkler H. Experimental and analytical studies of innovative prestressed concrete box-girder bridges. Mater Struct 2003;36(2):99–107.
[16] Chen XC, Li Z, Au FT, Jiang R. Flexural vibration of prestressed concrete bridges with corrugated steel webs. Int J Struct Stab Dyn 2016;16(10):1750023.
[17] Harris HG, Sabnis G. Structural modeling and experimental techniques. 2nd ed. Boca Raton: CRC Press; 1999.
[18] The Ministry of Transport of the People's Republic of China. General specifications for design of highway bridges and culverts. Beijing: China Communications Press; 2015.